Letters

IOP Publishing

Plasma Sources Science and Technology

Plasma Sources Sci. Technol. **30** (2021) 03LT04 (6pp)

https://doi.org/10.1088/1361-6595/abe728

Letter

Intrasheath electron dynamics in low pressure capacitively coupled plasmas

Máté Vass[1,2,*], Aranka Derzsi[2], Julian Schulze[1,3], and Zoltán Donkó[2]

[1] Department of Electrical Engineering and Information Science, Ruhr-University Bochum, D-44780, Bochum, Germany

[2] Institute for Solid State Physics and Optics, Wigner Research Centre for Physics, H-1121 Budapest, Konkoly-Thege Miklós str. 29-33, Hungary

[3] Key Laboratory of Materials Modification by Laser, Ion, and Electron Beams (Ministry of Education), School of Physics, Dalian University of Technology, Dalian 116024, People's Republic of China

E-mail: vass@aept.ruhr-uni-bochum.de

Received 15 December 2020, revised 26 January 2021
Accepted for publication 17 February 2021
Published 15 March 2021

Abstract

We present a detailed analysis of electron trajectories within the sheath regions of capacitively coupled plasmas excited by radio-frequency voltage waveforms at low pressures. Complex features inside the sheaths are identified in several physical quantities, which are sculptured by the trajectories of bouncing energetic electrons (predominantly ion induced secondary electrons) under the influence of the spatio-temporally varying electric field. Based on a systematic parameter variation the generation of the various features as a function of surface processes is explained and the trajectories of electrons of different origin are identified.

Keywords: capacitively coupled plasmas, charged particle dynamics, particle-in-cell simulations

(Some figures may appear in colour only in the online journal)

Capacitively coupled radio-frequency (RF) plasma sources are of great importance due to their numerous industrial applications [1–3]. Due to the complex nature of the underlying physical mechanisms, such as e.g. the coexistence of neutral and charged particles under nonequilibrium conditions, a description based on kinetic theory is necessary [4, 5], which is usually acquired based on numerical computer simulations [6, 7]. As the lightest charged particles in low temperature plasmas are electrons, understanding their kinetics and their interaction with the spatio-temporally varying electric field inside the plasma is of utmost importance, as they are primarily responsible for sustaining the plasma and for generating reactive neutrals via dissociation. Depending on the electron kinetics, distinct operation modes (such as the α- and γ-modes) and transitions between these exist in RF plasmas. The α-mode is associated with electron heating at the edge of the expanding sheath, while in the γ-mode secondary electrons ('γ-electrons') emitted from the electrodes and accelerated by the sheath electric field, cause significant ionization and increase the plasma density [8–11]. Mode transitions are intimately coupled with the electron energy distribution function [12].

The physics of low temperature plasmas is further enriched by the *non-local* character of the electron transport: in typical low-pressure settings the electric field usually varies in space along the free flights of the electrons, or varies in time between two collisions, which is intimately related to the electrons' interactions with the sheaths [13–15]. At low pressures, the electrons interacting with one sheath can reach the opposite sheath without undergoing many collisions, thus leading to a scenario where electrons 'bounce' back and forth between the two sheaths and *bounce resonance heating* can

* Author to whom any correspondence should be addressed.

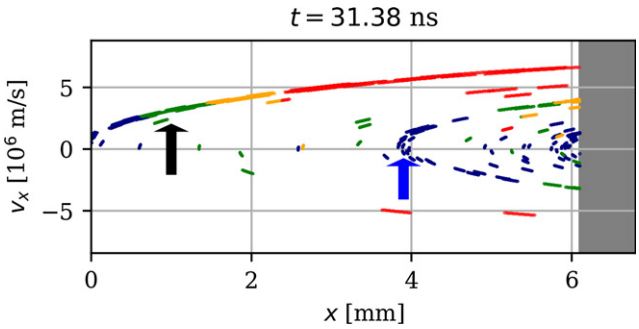

Figure 1. Configuration space of the electrons at $t = 31.38$ ns during sheath expansion within the RF-cycle. The powered electrode is at $x = 0$ and the grey region marks the plasma bulk. Note (i) the parabolic line from the origin that corresponds to γ-electrons emitted from the electrode and fly towards the center (marked by the black arrow) and (ii) the pronounced turning point of a *group* of electrons at ≈4 mm inside the sheath (marked by the blue arrow). The 'traces' of individual electrons correspond to a time window of ≈0.14 ns. (A movie, covering the full RF period is available as supplementary material.) The colors correspond to different energies: navy: 0–20 eV, green: 20–40 eV, orange: 40–60 eV, red: ⩾60 eV.

occur [16, 17]. As in reality there is an electric field even outside the sheath region, which is predominantly an ambipolar electric field [18, 19], low energy electrons, which are usually 'trapped' within the discharge, can effectively be 'heated' under such resonant conditions by the ambipolar field as well [20]. The spatio-temporally resolved non-local dynamics of electrons, especially that of secondary electrons, at low pressures as a consequence of their interaction with the boundary surfaces and with the RF modulated sheaths is not fully understood. Highly energetic electrons, which can traverse through the whole discharge, called *beam electrons* have been the subject of numerous research works [21–24]. Fu *et al* [25] investigated the kinetic behaviour of highly energetic γ-electrons within the bulk (*high-energy ballistic electrons*) and their effect on different plasma parameters. They conducted test particle simulations using the particle-in-cell/Monte Carlo collisions (PIC/MCC) method to trace electrons and determined their 'bouncing' between the sheath boundaries. Wang *et al* revealed the origin of specific structures in the energy distribution of electrons reaching the electrodes [26].

In previous works, studies of the electron-sheath interaction have mostly been restricted to thermal electrons that interact with the sheath stochastically at different times throughout the RF period [1, 2] and to beam electrons generated by sheath expansion heating at the opposite electrode [16, 17, 21]. Due to their relatively low energy such electrons do not penetrate deeply into the sheath and have not been found to cause significant intrasheath phenomena. Thus, the sheath is typically modelled as a hard wall for electrons. As secondary electrons can obtain much higher energies, since they are generated at the electrode surface and can gain energy according to the full sheath potential, they can penetrate much more deeply into the opposite sheath after traversing the bulk collisionlessly. For such electrons the sheath edge is no longer a hard wall and significant intrasheath dynamics can occur, which have not been analysed before.

In this letter, we identify 'features' observed in various physical properties of the plasma inside the sheaths and explain them by the complex motions of different types of (not exclusively γ-) electrons. The results reveal the complex intrasheath dynamics of electrons and, therefore, represent a step towards understanding the dynamics of energetic electrons in low temperature plasmas.

Penetration of high energy electrons deep into the sheath from the plasma side is clearly revealed in figure 1 that shows electron trajectories in the $(x - v_x)$ configuration space in an argon plasma at $p = 1$ Pa, assuming plane parallel electrodes with a gap of $L = 50$ mm, established by an RF voltage $\Phi(t) = \Phi_0 \cos(2\pi f t)$ with an amplitude of $\Phi_0 = 150$ V, at a frequency of $f = 13.56$ MHz. These conditions are referred to as the 'base case' in the following. The results are obtained from PIC/MCC simulation of the discharge [27–29]. The model assumes two constant surface coefficients: an elastic electron reflection probability, $R = 0.2$, and an ion-induced secondary electron emission coefficient, $\gamma = 0.4$.

The penetration of the fast electrons into the sheaths—made possible by a 'soft' boundary—gives rise to various curved features that can be observed when analysing the spatio-temporal distribution of several physical quantities related to the electrons, as illustrated in figures 2(a)–(d) for the base case specified above: the mean energy, $\langle\varepsilon\rangle$ (a), longitudinal temperature, T_{xx} (b), density, n_e (c) and normalised density gradient, $\nabla n_e/n_e$ (d). The mean energy and density show very similar structures within the sheath together with the longitudinal temperature, whereas in the latter there is a difference in the region between ≈20–45 ns in the RF-cycle (near the electrode). The reason for this is, that in this temporal domain only a few electrons, coming from the center of the discharge, can penetrate deep into the sheath. Thus, predominantly γ-electrons (emitted from the adjacent electrode) will contribute to the mean energy and the temperature. The definition of the temperature is $T_{xx} = m_e(\langle v_x^2\rangle - u_x^2)$, where m_e is the electron mass, v_x and u_x are the velocity of an electron and the mean velocity of the electrons in the x-direction, respectively. Thus, it is proportional to the variance of the electrons' velocity, which, for the γ-electrons, is low, as they are emitted from the electrode with the same energy and need many collisions before their velocities are randomised. This, on the other hand, does not mean, that their mean energy, defined by $\langle\varepsilon\rangle = \frac{m_e}{2}\langle v_x^2 + v_y^2 + v_z^2\rangle$, cannot be large.

As the normalised electron density gradient shows the curved features most clearly, we will concentrate on this quantity from now on to identify the reason for the appearance of the different structures. The enumerated features identified in figure 2(d) are the ones to be explained. As a first step, the sensitivity of these structures on the operating conditions is addressed, as shown in figures 2(d)–(f). Panel (d) corresponds to the base case. As the pressure is increased [panels (e)–(f)], the features gradually disappear: first 4, 5 and 6 already at 2 Pa, and then 1 and 3 with only feature 2 remaining at 5 Pa. As ultimately these curved features are caused by the motion of electrons, the increase in pressure means that electrons undergo more collisions and, thus, their 'collective' motion is inhibited

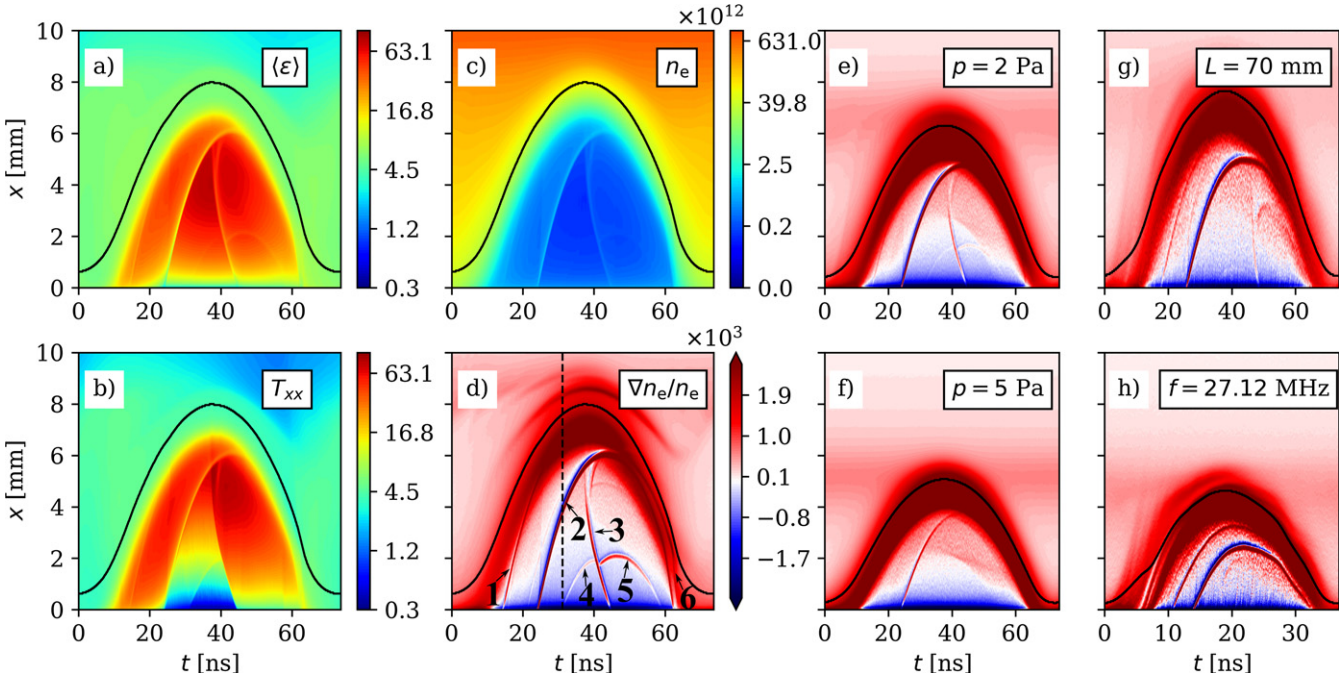

Figure 2. Mean energy [eV], $\langle\varepsilon\rangle$, (a), longitudinal electron temperature, T_{xx} [eV], (b), density [m^{-3}] (c) and normalised density gradient [m^{-1}] (d) of the electrons for the base case ($p = 1$ Pa, $L = 50$ mm, $f = 13.56$ MHz), and the effects of parameter variations on the normalised electron density gradient (e)–(h). The parameter that differs from the value in the base case is noted in the upper right corners of the panels. The dashed black line in panel (d) corresponds to the time instance shown in figure 1. The numbers and the corresponding arrows indicate the features investigated. The solid black lines indicate the sheath edge [30]. The plots show only the vicinity of the powered electrode situated at $x = 0$. The color scale of panel (d) applies for panels (e)–(h).

at higher pressures. In other words, the complex features are caused by electrons reaching the vicinity of the powered electrode, which is less likely to happen when the pressure is increased. By increasing the gap length, L [panel (g)], the features get shifted in time, due to the fact, that the electrons need more time to traverse a longer gap. The frequency variation [panel (h)] results in a smaller sheath width, which is attributed to the higher plasma density. Features 1 and 2 can be identified in panel (h), but the others are not present. This, as we shall see, is due to the fact that in order for a given trajectory to be formed, it matters in which phase of the sheath expansion/collapse the electron arrives at the instantaneous sheath edge.

Based on this, one can infer that the complex features in the figures above do not correspond to individual electron trajectories, but rather to the envelope of these, i.e. it is the ensemble of turning points of incoming electrons (cf figure 1) which together give rise to the features. This necessitates two remarks: (i) given this predicate, it is more understandable why we see a difference between figures 2(a) and (b): as many electrons that reach the sheath region will turn back giving rise to feature 2 in panel (d), in the region below feature 2 predominantly γ-electrons will be present, which, as elucidated above, give rise to a smaller electron temperature. (ii) The features identified in the normalised electron density gradient shown in figure 2(d) all have a negative (blue) and a positive (red) side. This can be explained by the fact, that at the turning points of the electrons the electron density is locally increased, which (as seen in figure 2(d)). This causes a positive edge in the gradient of the electron density at the side of the powered electrode, and a negative one in the other direction.

As γ-electrons reach much higher energies than the electrons born outside the sheath, they are the primary suspects for the generation of the complex features. Following their trajectories aids the explanations of these features. A sketch of the principal electron trajectories is shown in figure 3: green circles denote γ-electrons, blue circles bulk (i.e. 'born in the bulk') electrons. Whenever an electron reaches the electrode surface, it undergoes a reflection from the electrode surface with a probability R. The ends of the trajectories (the arrowheads) correspond to the approximate place/time where the electrons turn back inside the sheath at the powered (bottom) electrode.

Our approach is to run simulations with every possible combination of the surface processes: we can have secondary electron emission on either electrodes, both or none (controlled by the γ-coefficient, having a value of 0 or 0.4), and similarly with the elastic electron reflection (controlled by the R coefficient, having a value of 0 or 0.2), which has already been applied in e.g. [31], albeit with a different goal compared to

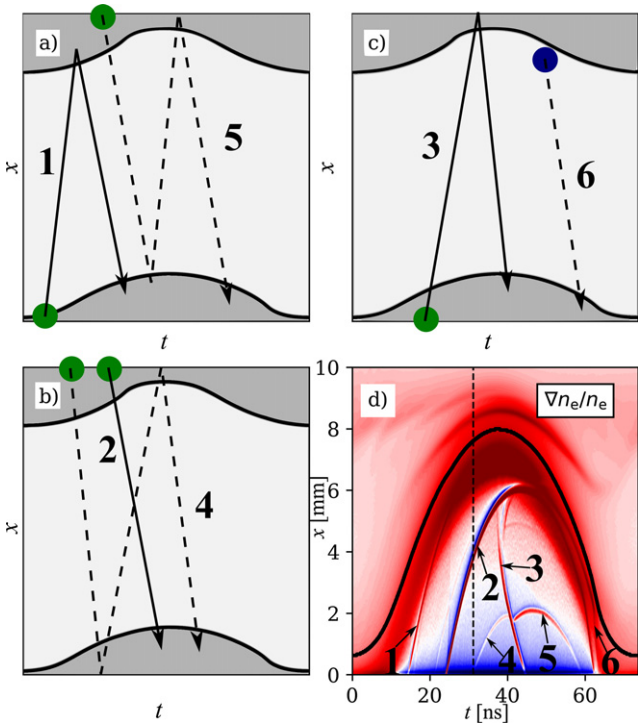

Figure 3. Sketch of principal electron trajectories aiding the explanations of the features identified and enumerated in figure 2(d). Green circles denote γ-electrons, blue circles stand for bulk electrons. The powered and grounded electrodes of the discharge are situated at the bottom and at the top of the graphs, respectively. Dark grey regions: sheath domains. Light grey regions: bulk. Thick black lines: sheath edges. For easier legibility figure 2(d) is reproduced in panel (d).

ours. For brevity and notational simplicity, 'bottom' and 'top' electrode will be used instead of powered/grounded. The results obtained this way for the base case are shown in figure 4.

Table 1 summarizes the appearances of the various features, by listing the numbers assigned to the features in figures 2(d) and 4(a).

Based on this table, it can readily be identified what surface process on either electrode is needed to generate the given pattern. In principle, this approach can be generalised to more than two surface processes, including e.g., secondary electron emission due to electron bombardment of the electrodes [32, 33].

Invoking figure 3, the features are identified as follows:

- Feature 1 (figure 3(a)) is present only in the γ bottom column, i.e. it is caused by secondary electrons born at the bottom electrode. As the feature is present irrespective of the presence of electron reflection, it means, that a γ-electron born at the bottom electrode traverses the whole discharge, is reflected by the opposing (top) sheath and flies back to the bottom electrode again. This can happen, as taking a γ-electron having an average energy of $\approx$75 eV, it can traverse the gap of 50 mm in $\approx$10 ns.
- Feature 2 (figure 3(b))—as it is present in the γ top column, it is caused by γ-electrons born at the top electrode, accelerated by the sheath electric field and reaching the bottom sheath where they are turned back.
- Feature 3 (figure 3(c))—as it is present in the γ bottom and R top panels, the feature is proven to be generated by those γ-electrons, which are born at the bottom electrode, traverse the discharge, reach the opposite electrode where they get reflected, and come back to the bottom sheath again.
- Feature 4 (figure 3(b)) is not among the panels discussed before, which means, that it has to be a multiple reflection-caused feature. It can only be found in the γ top column with both electrodes having nonzero reflection coefficients (R both row). This means, that this feature is caused by electrons born at the top electrode, reflected twice by either electrodes before turning back in the bottom sheath region.
- Feature 5 (figure 3(a)) is again a multiple reflection-caused feature, because it is found in the γ top column and the R top row, which means the electron is born at the top electrode, but also reflected by it. The only way it can happen is, if it is first reflected by the bottom sheath and then the top electrode.
- Feature 6 (figure 3(c)) is the only structure which appears in the γ none column, and is not sensitive to reflections. Thus, it is caused by electrons generated within the plasma bulk that reach the bottom sheath.

We note that the intrasheath features observed in figure 2 do not cause any significant modification of the spatio-temporal distribution of the potential inside the sheath, i.e. their weak effects on the electron density inside the sheath (shown in figure 2(c)) do not modify the sheath electric field significantly. Thus, the observed intrasheath features are a sole and direct consequence of the electron motion rather than the effect of a modification of the electric field inside the sheath.

In summary, the complex dynamics of fast electrons were analysed in low pressure capacitively coupled plasmas via PIC/MCC simulations. Prominent features in a number of physical parameters were found inside the sheath regions. We have successfully associated these features with distinct mechanisms of energetic electron generation [1, 2, 8, 11, 21] and the motion of these electrons in the spatio-temporally varying electric field as well as their reflection at boundary surfaces and sheaths. It was found that they primarily originate from energetic ion induced secondary electrons, as these have a high enough energy to be able to penetrate deeply into the sheath region at the opposite electrode. It was inferred that the features do not correspond to trajectories, but are envelopes of the turning points of these electrons within the sheath region. Each feature was associated with particular groups of energetic electrons and their non-local dynamics in the plasma. This was revealed by a procedure where the electrode surface processes were turned on/off (by assuming nonzero/zero values for the surface coefficients) and all possible combinations have been scanned. This approach enables a deeper understanding of the complex and non-local spatio-temporal dynamics of energetic electrons in technological plasmas.

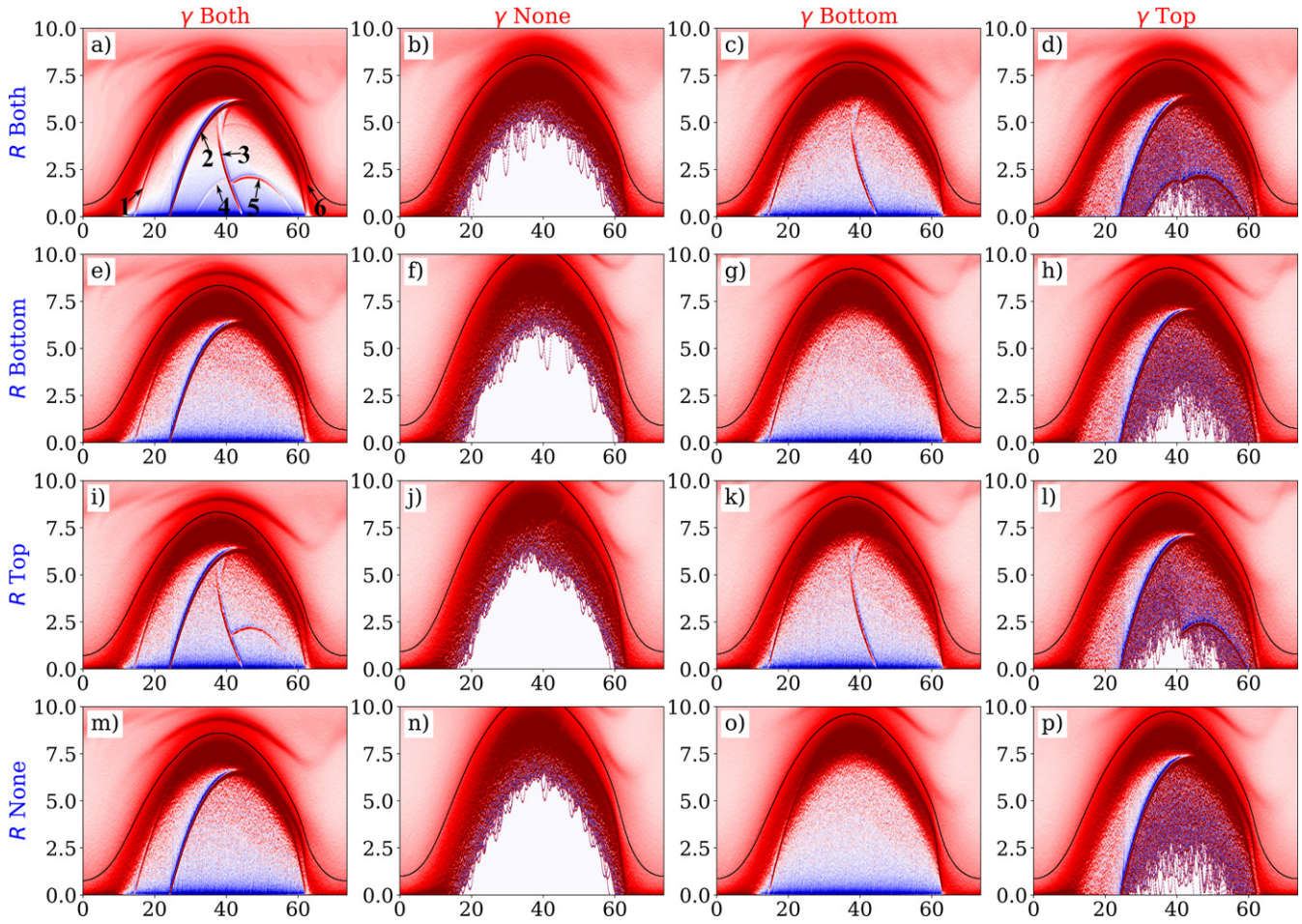

Figure 4. Features under different electrode surface conditions. The panels show the normalized electron density gradient. The presence/absence of the electron reflection process (rows) and the secondary electron emission process (columns) are indicated by the keywords 'both', 'none', 'Top' and 'Bottom', which refer to the electrodes. The Bottom electrode is situated at $x = 0$. For clarity, axis labels and colorbars are omitted, they agree with that of figure 2(d).

Table 1. Appearances of the various features.

	γ both	γ none	γ bottom	γ top
R both	1–6	6	1, 3, 6	2, 4, 5, 6
R bottom	1, 2, 6	6	1, 6	2, 6
R top	1, 2, 3, 5, 6	6	1, 3, 6	2, 5, 6
R none	1, 2, 6	6	1, 6	2, 6

Data availability statement

The data that support the findings of this study are available upon reasonable request from the authors.

Acknowledgments

The authors acknowledge funding from the German Research Foundation in the frame of the project, 'Electron heating in capacitive RF plasmas based on moments of the Boltzmann equation: from fundamental understanding to knowledge based process control' (No. 428942393), via SFB TR 87, project C1, and from the Hungarian National Office for Research, Innovation, and Technology (NKFIH), via grants K134462 and FK128924.

ORCID iDs

Máté Vass https://orcid.org/0000-0001-9865-4982
Aranka Derzsi https://orcid.org/0000-0002-8005-5348
Julian Schulze https://orcid.org/0000-0001-7929-5734
Zoltán Donkó https://orcid.org/0000-0003-1369-6150

References

[1] Lieberman M A and Lichtenberg A J 2005 *Principles of Plasma Discharges and Materials Processing* (New York: Wiley)
[2] Chabert P and Braithwaite N 2011 *Physics of Radio-Frequency Plasmas* (Cambridge: Cambridge University Press)
[3] Makabe T and Petrovic Z L 2014 *Plasma Electronics: Applications in Microelectronic Device Fabrication* vol 26 (Boca Raton, FL: CRC Press)
[4] Alves L L, Bogaerts A, Guerra V and Turner M M 2018 *Plasma Sources Sci. Technol.* **27** 023002
[5] Kolobov V I 2013 *Phys. Plasmas* **20** 101610
[6] Verboncoeur J P 2005 *Plasma Phys. Control. Fusion* **47** A231
[7] Tejero-del-Caz A, Guerra V, Gonçalves D, da Silva M L, Marques L, Pinhão N, Pintassilgo C D and Alves L L 2019 *Plasma Sources Sci. Technol.* **28** 043001

[8] Belenguer P and Boeuf J P 1990 *Phys. Rev.* A **41** 4447–59
[9] Kawamura E, Lichtenberg A J and Lieberman M A 2008 *Plasma Sources Sci. Technol.* **17** 045002
[10] Garner A L, Meng G, Fu Y, Loveless A M, Brayfield R S and Darr A M 2020 *J. Appl. Phys.* **128** 210903
[11] Daksha M, Derzsi A, Wilczek S, Trieschmann J, Mussenbrock T, Awakowicz P, Donkó Z and Schulze J 2017 *Plasma Sources Sci. Technol.* **26** 085006
[12] Kim H C and Lee J K 2004 *Phys. Rev. Lett.* **93** 085003
[13] Tsendin L D 2010 *Phys. -Usp.* **53** 133–57
[14] Kaganovich I D 2002 *Phys. Rev. Lett.* **89** 265006
[15] Sheehan J P, Hershkowitz N, Kaganovich I D, Wang H, Raitses Y, Barnat E V, Weatherford B R and Sydorenko D 2013 *Phys. Rev. Lett.* **111** 075002
[16] Liu Y X, Zhang Q Z, Jiang W, Hou L J, Jiang X Z, Lu W Q and Wang Y N 2011 *Phys. Rev. Lett.* **107** 055002
[17] Liu Y-X, Zhang Q-Z, Liu J, Song Y-H, Bogaerts A and Wang Y-N 2012 *Appl. Phys. Lett.* **101** 114101
[18] Schulze J, Derzsi A, Dittmann K, Hemke T, Meichsner J and Donkó Z 2011 *Phys. Rev. Lett.* **107** 275001
[19] Schulze J, Donkó Z, Lafleur T, Wilczek S and Brinkmann R P 2018 *Plasma Sources Sci. Technol.* **27** 055010
[20] Park G Y, You S J, Iza F and Lee J K 2007 *Phys. Rev. Lett.* **98** 085003
[21] Schulze J, Heil B G, Luggenhölscher D, Mussenbrock T, Brinkmann R P and Czarnetzki U 2008 *J. Phys. D: Appl. Phys.* **41** 042003
[22] Wilczek S, Trieschmann J, Schulze J, Schuengel E, Brinkmann R P, Derzsi A, Korolov I, Donkó Z and Mussenbrock T 2015 *Plasma Sources Sci. Technol.* **24** 024002
[23] Berger B, You K, Lee H-C, Mussenbrock T, Awakowicz P and Schulze J 2018 *Plasma Sources Sci. Technol.* **27** 12LT02
[24] Vass M, Wilczek S, Lafleur T, Brinkmann R P, Donkó Z and Schulze J 2020 *Plasma Sources Sci. Technol.* **29** 085014
[25] Fu Y, Zheng B, Wen D-Q, Zhang P, Fan Q H and Verboncoeur J P 2020 *Plasma Sources Sci. Technol.* **29** 09LT01
[26] Wang L, Hartmann P, Donkó Z, Song Y H and Schulze J Plasma Sources Sci. Technol. submitted.
[27] Donkó Z 2011 *Plasma Sources Sci. Technol.* **20** 024001
[28] Verboncoeur J P, Langdon A B and Gladd N T 1995 *Comput. Phys. Commun.* **87** 199–211
[29] Matyash K, Schneider R, Taccogna F, Hatayama A, Longo S, Capitelli M, Tskhakaya D and Bronold F X 2007 *Contrib. Plasma Phys.* **47** 595–634
[30] Brinkmann R P 2007 *J. Appl. Phys.* **102** 093303
[31] Sun A, Becker M M and Loffhagen D 2018 *Plasma Sources Sci. Technol.* **27** 054002
[32] Horváth B, Schulze J, Donkó Z and Derzsi A 2018 *J. Phys. D: Appl. Phys.* **51** 355204
[33] Horváth B, Daksha M, Korolov I, Derzsi A and Schulze J 2017 *Plasma Sources Sci. Technol.* **26** 124001